JACS
JOURNAL OF THE AMERICAN CHEMICAL SOCIETY
Communication
pubs.acs.org/JACS

Probing Redox Photocatalysis of Trapped Electrons and Holes on Single Sb-doped Titania Nanorod Surfaces

Weilin Xu,[†,‡] Prashant K. Jain,[†,‡,§] Brandon J. Beberwyck,[‡,∥] and A. Paul Alivisatos*,[†,‡,∥]

[†]Department of Chemistry, University of California, Berkeley, California 94720, United States
[‡]Materials Sciences Division, Lawrence Berkeley National Laboratory, Berkeley, California 94720, United States
[§]Miller Institute for Basic Research in Science, University of California, Berkeley, California 94720, United States
[∥]Department of Materials Science and Engineering, University of California, Berkeley, California 94720, United States

S *Supporting Information*

ABSTRACT: We used a fluorogenic reaction to study in conjunction the photocatalytic properties for both active sites (trapped photogenerated electrons and holes) on individual Sb-doped TiO_2 nanorods with single-molecule fluorescence microscopy. It was found that active sites around trapped holes show higher activity, stronger binding ability, and a different dissociation mechanism for the same substrate and product molecules in comparison with the active sites around trapped electrons. These differences could be elucidated by a model involving the charged microenvironments around the active sites.

Since the discovery of photoinduced decomposition of water on a TiO_2 electrode,[1] TiO_2-based photocatalysts have attracted wide attention.[2−8] When TiO_2 is exposed to light of energy greater than the band-gap energy, electrons are excited from its valence band into the conduction band to form spatially separated electron/hole (e^-/h^+) pairs by light absorption. These photogenerated charge carriers can either recombine or become trapped and react with electron donors or acceptors adsorbed on the surface of the photocatalyst.[9] As shown in Scheme 1A, in an aqueous environment, photogenerated electrons are trapped by adsorbed oxygen, generating bound superoxide anion radicals ($O_2^{-\bullet}$), and photogenerated holes are trapped by adsorbed water or hydroxyl (OH^-), generating bound hydroxyl radicals ($OH^\bullet$).[2−4] This scheme has been extensively validated by the detection of these two radicals during the TiO_2 photocatalytic reactions at the ensemble[10−18] and single-molecule[19−21] levels. Photochemical reactions and photocatalysis are known to be based on these two basic radicals $h^+/OH^\bullet$ and $e^-/O_2^{-\bullet}$ or their associated catalytic sites, although the nature of these two basic catalytic sites has not been clarified.[22,23]

Scheme 1. (A) Scheme for the Generation of Photogenerated Electron/Hole Pairs and Subsequent Trapping by the Chemicals Adsorbed on a TiO_2-Based Photocatalyst Surface To Form Two Radicals; (B) Reactions of Hydroxyl and Superoxide Anion Radicals with Amplex Red To Form the Fluorescent Product Resorufin

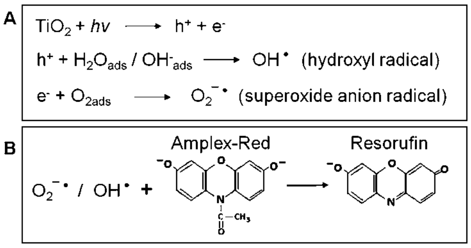

Here, on the basis of the fact that both of these radicals or active sites $h^+/OH^\bullet$ and $e^-/O_2^{-\bullet}$ can react oxidatively with nonfluorescent amplex red to form the fluorescent product resorufin (Scheme 1B),[24] the two photocatalytic redox reactions were studied in conjunction using the same single-molecule detection scheme. We have obtained new insight into the active sites involved in $h^+/OH^\bullet$ and $e^-/O_2^{-\bullet}$, which can be elucidated by a model involving the charged microenvironments around the active sites.

Anatase TiO_2 nanorods were synthesized according to the literature[25] and then doped with antimony (Sb) [for details, see the Supporting Information (SI)]. Transmission electron microscopy (TEM) showed that the length and diameter of these Sb-doped TiO_2 nanorods were ~42 nm and ~2.4 nm, respectively (Figure 1). Diffuse reflectance and absorbance spectroscopy (Figure 2A) revealed that the band gap of the unmodified TiO_2 nanorods (white) was ~3.3 eV, while the onset of the optical absorption of the Sb-doped TiO_2 nanorods (yellowish) was lowered to ~2 eV (~600 nm). Since Sb doping on TiO_2 could not lead to the formation of oxygen vacancies,[26] this sub-band-gap red absorption in the Sb-doped TiO_2 nanocrystals is likely due to intraband transitions.[5,27]

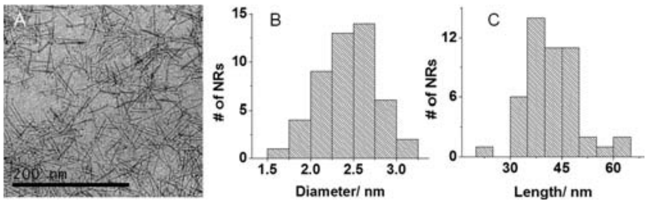

Figure 1. (A) TEM image of Sb-doped TiO_2 nanorods. (B) Diameter distribution (average 2.4 nm). (C) Length distribution (average 42 nm).

For single-molecule reaction experiments, individual Sb-doped TiO_2 nanorods were immobilized on a quartz slide

Received: October 24, 2011
Published: February 16, 2012

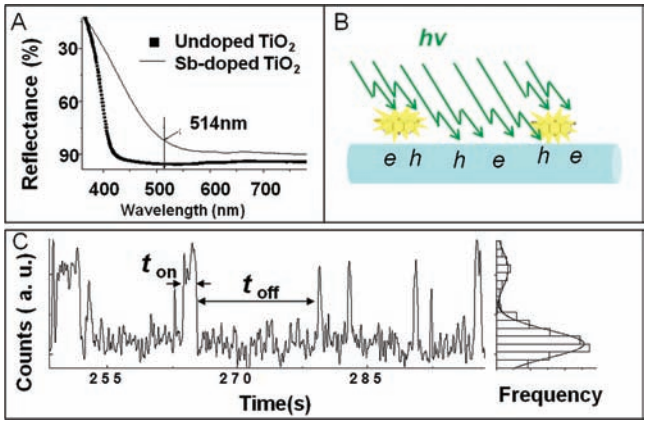

Figure 2. (A) Diffuse reflectance spectra of undoped and Sb-doped TiO_2 nanorods. (B) Scheme showing excitation of both the Sb-doped TiO_2 nanorod and the fluorescent product molecules formed on its surface using the same visible-light source. (C) (left) Segment of a typical fluorescence trajectory from a single-molecule experiment with 1.0 μM amplex red, 20 mM DMSO, and 50 mM phosphate buffer (pH 7.3); (right) histogram distribution of the fluorescence intensity on the segment of the trajectory shown at the left.

surface. The substrate amplex red (the reductant in the redox system) in phosphate buffer solution was flowed over the surface with nanorods sandwiched within a flow cell assembly as described previously.[28] In this redox system, the oxidants (bound $OH^{\bullet}$ or $O_2^{-\bullet}$ radicals) are formed in situ on the surface of the nanocatalyst and then undergo a redox reaction with amplex red (Scheme 1). To study purely dopant-induced photon absorption and subsequent photocatalysis,[5,29] we excited the nanorods with a green laser with $\lambda = 514$ nm, well below the band gap of undoped TiO_2. The green laser was used both to excite Sb-doped TiO_2 nanorods to create photogenerated e^-/h^+ pairs and to image fluorescent product resorufin molecules formed by the photocatalysis (Figure 2B). This fact was also validated by ensemble control experiments (see the SI).

To study the reactivity of bound $OH^{\bullet}$ radicals formed from trapped holes solely, superoxide dismutase (SOD) (200 units/mL) was used to quench $O_2^{-\bullet}$ radicals formed on the Sb-doped TiO_2 nanorod surfaces (Figure S1 in the SI).[30] Similarly, for the study of $O_2^{-\bullet}$ anion radicals, dimethyl sulfoxide (DMSO) (20 mM) was used to quench $OH^{\bullet}$ radicals formed on the Sb-doped TiO_2 nanorod surfaces.[31] We were thus able to study separately the reactivities of the two radicals or active sites $h^+/OH^{\bullet}$ and $e^-/O_2^{-\bullet}$ on the surface of individual Sb-doped TiO_2 nanorods by observing the individual fluorescent product formation locally with a total internal reflection fluorescence (TIRF) microscope and single-turnover resolution. We recorded movies of fluorescence intensity bursts resulting from the formation of single resorufin molecules in the redox reactions. Figure 2C shows a typical time trajectory of the fluorescence intensity obtained from a single-molecule catalytic movie using DMSO as the quencher. The trajectory contains two-state off/on signals. The digital, two-state nature of these fluorescence trajectories indicates that each burst comes from a single product molecule. Otherwise, the trajectory would have a variable number of intensity states depending on the number of molecules.[28] No digital signals were observed from the Sb-doped TiO_2 surface when both radical quenchers were added to the substrate solution. No digital signals were observed on pure TiO_2 or in the absence of substrate. Therefore, we attribute the single-product fluorescence bursts to the oxidation of amplex red to form resorufin by either one of these two radicals rather than the photogenerated electrons or holes.

In the single-molecule trajectories (Figure 2C), each sudden intensity increase corresponds to the oxidative formation of a single product molecule at a reactive site on a Sb-doped TiO_2 nanorod. Here the reactive site on the Sb-doped TiO_2 could be defined as a site on which an e^-/h^+ pair formed by an absorbed photon is trapped by O_{2ads} or H_2O_{ads}/OH^-_{ads} to form reactive radicals. Accordingly, we classify active sites on TiO_2-based photocatalysts into two types: $h^+/OH^{\bullet}$ and $e^-/O_2^{-\bullet}$. Sudden intensity decreases in trajectories could be due to (1) photobleaching of product molecules; (2) fluorescence blinking of product molecules; (3) product dissociation from the reactive site; or (4) further oxidation of the fluorescent product resorufin to form nonfluorescent resazurin. Under similar laser excitation and buffer conditions, control experiments with resorufin but no quenchers on the Sb-doped TiO_2 surface showed that the average blinking on time was ~16 s (Figure S2) and the average photobleaching time was even longer than 16 s. Both of them are much longer than the average t_{on} in the fluorescence trajectories (typically <1 s). Also, if further oxidation of resorufin by either of the two radicals could occur easily on the Sb-doped TiO_2 surface, we could not get such long average on times. Therefore, statistically, photoblinking, photobleaching, or further oxidation of resorufin to resazurin could not be main contributors to the sudden intensity drops. We therefore attribute the sudden decreases in intensity to the dissociation of product from the surface of the nanorod (see the SI).

In the single-molecule fluorescence trajectories (Figure 2C), the waiting times τ_{off} and τ_{on} are the two important characteristic durations. Resolving them enabled us to probe the kinetic mechanism of the reactions in two separate stages: τ_{off} is the waiting time before the formation of a fluorescent product on the Sb-doped TiO_2 nanorod, and τ_{on} is the characteristic time for which persistent emission is exhibited, which should be related to the rate of dissociation of the product molecule from the nanorod surface as discussed above.[32]

For both $OH^{\bullet}$ and $O_2^{-\bullet}$ radicals, the product formation rate, $\langle\tau_{off}\rangle^{-1}$, was dependent on substrate concentration [S] (Figure 3A), as expected. Here, because of the huge number of photogenerated e^-/h^+ pairs and the high concentration of H_2O/OH^- and O_2 in the (air-saturated) buffer system, we assume that the concentrations of these two radicals formed according to Scheme 1A on Sb-doped TiO_2 surfaces were much higher than the substrate concentration and remained fairly constant during the course of a whole study.[6,7]The dependence of the product formation rate on

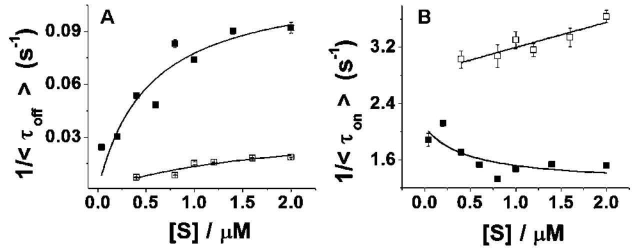

Figure 3. Dependence of (A) $\langle t_{off}\rangle^{-1}$ and (B) $\langle t_{on}\rangle^{-1}$ on the concentration of the substrate, amplex red, with (■) $OH^{\bullet}$ or (□) $O_2^{-\bullet}$ as the oxidant. Each point was obtained from the average of more than 50 individual nanoparticles. Error bars are standard errors of the mean. Solid lines are fits to the data using (A) eq 1 and (B) eq 2.

Table 1. Results of the Fits to Equations 1 and 2 for the Reactions on the Two Catalytic Sites with $OH^\bullet$ and $O_2^{-\bullet}$ Radicals as Oxidants

active site	K_1 (μM^{-1})	γ_{eff} (s^{-1})	γ_2 (s^{-1})	γ_3 (s^{-1})	K_2 (μM^{-1})
$h^+/OH^\bullet$	1.9 ± 0.8	0.12 ± 0.02	1.26 ± 0.36	2.1 ± 0.2	2.1 ± 1.3
$e^-/O_2^{-\bullet}$	0.55 ± 0.33	0.04 ± 0.01	55 ± 11	2.8 ± 0.1	0.007 ± 0.002

[S] can be then described by the Langmuir−Hinshelwood equation (eq 1)[28]

$$\left\langle \tau_{off} \right\rangle^{-1} = \frac{\gamma_{eff} K_1 [S]}{1 + K_1 [S]} \tag{1}$$

where K_1 is the equilibrium adsorption constant for the substrate on Sb-doped TiO_2 nanorods and γ_{eff} the net reactivity of the individual nanorod. By fitting the data with eq 1, as shown in Figure 3A, the values of K_1 and γ_{eff} for the reactions with the two different radicals as oxidants were obtained. Interestingly, as shown in Table 1, K_1 and γ_{eff} for the reactions with $OH^\bullet$ as the oxidant are 4 and 3 times larger, respectively, than those for the reactions with $O_2^{-\bullet}$ as the oxidant. The large difference in the value of K_1 probably arises because the positively charged (or electrophilic) microenvironment around trapped holes can enhance the adsorption of negatively charged substrate molecules while the negatively charged microenvironment around trapped photogenerated electrons minimizes the adsorption of the negatively charged substrate molecules. The higher value of γ_{eff} for the reaction with $OH^\bullet$ as the oxidant on an individual nanorod indicates that the reactivity of $OH^\bullet$ is 2 times higher than that of $O_2^{-\bullet}$, which is consistent with a previous observation in an ensemble experiment.[31] The oxidative reactivity difference also could be attributed in part to the fact that the electrophilic microenvironment around trapped holes ($h^+/OH^\bullet$) makes the electron transfer from the substrate to the reactive site easier in comparison with that allowed by the nucleophilic microenvironment around trapped electrons. The other possible reason for the γ_{eff} difference could be a higher surface concentration of $OH^\bullet$ than $O_2^{-\bullet}$, since γ_{eff} contains a contribution from the oxidant concentration.[32]

For the product dissociation step (Figure 3B), the product dissociation rates for the reactions with these two different radicals as oxidants were also dependent on [S], indicating that substrate molecules were also involved in the product dissociation process. The total product dissociation rate can be described by eq 2:[32]

$$\left\langle \tau_{on} \right\rangle^{-1} = \frac{\gamma_2 K_2 [S] + \gamma_3}{1 + K_2 [S]} \tag{2}$$

in which γ_2 is the rate constant for product dissociation in the substrate-assisted pathway, γ_3 is the rate constant for direct product dissociation, and $K_2 = \gamma_1/(\gamma_{-1} + \gamma_2)$, where γ_1 the rate constant for the substitution of a product molecule by a substrate molecule on a reactive site and γ_{-1} is the rate constant for the reverse process.

Interestingly, for the reactions on the $h^+/OH^\bullet$ active sites, the product dissociation was slow and proceeded mainly through the direct product dissociation pathway ($\gamma_2 = 1.26\ s^{-1}$, $\gamma_3 = 2.1\ s^{-1}$). The product dissociation rate (■ curve in Figure 3B) decreased with increasing substrate concentration because of the smaller γ_2 value, which reflects the fact that more product molecules dissociate through the slower substrate-assisted pathway at higher substrate concentrations. For the reactions on the $e^-/O_2^{-\bullet}$ active sites, the product dissociation was much faster and proceeded mainly through the substrate-assisted pathway ($\gamma_2 = 55\ s^{-1}$, $\gamma_3 = 2.8\ s^{-1}$). The product dissociation rate (□ curve in Figure 3B) increased with increasing substrate concentration because of the smaller γ_3, which reflects the fact that more product molecules dissociate through the faster substrate-assisted pathway at higher substrate concentrations. The slower dissociation process of the product on $h^+/OH^\bullet$ sites could be attributed to the attraction between the negatively charged product molecule and the positively charged microenvironment around the trapped holes. The faster product dissociation around $e^-/O_2^{-\bullet}$ may be related to the repulsive force between the negatively charged product molecule and the negatively charged microenvironment around the trapped electrons. The value of K_2 is larger for the $h^+/OH^\bullet$ active sites (2.1 μM^{-1}) than for the $e^-/O_2^{-\bullet}$ active sites (0.007 uM^{-1}). This possibly indicates that the product molecule (which contains one negatively charged group) can be more easily substituted by a substrate molecule (which contains two negatively charged groups) at a $h^+/OH^\bullet$ active site in comparison with the similar substitution process at an $e^-/O_2^{-\bullet}$ active site.

The photocatalytic effect of the Sb dopant has been demonstrated previously.[33] Although the mechanism of visible-light photocatalytic activity of Sb-doped TiO_2 is not definitively known, it is believed that Sb doping creates an effective shallow trap for charge carriers.[33] As an electron donor, Sb^{4+} can easily donate one electron to Ti^{4+} ($3d^0$, which is above or at the edge of the conduction band) to form Ti^{3+} ($3d^1$, which is localized in the band gap well below the bottom of the conduction band).[27] The Sb^{5+} ions can be substituted into the TiO_2 lattice to create [O−Ti−O−Sb, Ti−O−Sb−O] sites.[34] Upon excitation with green light, as shown in the optical absorption spectra in Figure 2A, electrons are excited from oxygen atoms in the conduction band, probably to the Ti 3d orbitals, and are further trapped by adsorbed O_2 to produce $O_2^{-\bullet}$ radicals. The photogenerated holes are trapped by adsorbed H_2O or OH^- to produce $OH^\bullet$ radicals bound to the surface.[13,35] These trapped electrons ($e^-/O_2^{-\bullet}$) or holes ($h^+/OH^\bullet$) react with the nearby adsorbed substrate molecules, as shown in Scheme 1. As a result of hole trapping, the active sites around trapped holes are on average positively charged, while the active sites around trapped electrons are negatively charged. The differently charged microenvironments eventually decide the reactive properties of these two types of active sites. It is possible the Sb doping influences the substrate binding. It has previously been found with noncontact atomic force microscopy that under certain conditions, Sb-rich nanoclusters form on TiO_2 surfaces as a result of surface segregation of Sb.[26] Here, however, we were unable to see Sb-rich nanoclusters on the TiO_2 nanorod surfaces directly using high-resolution TEM or energy-filtered TEM, possibly because of the formation of only few-atom-sized clusters or a homogeneous distribution of dopant on the entire surface.

In conclusion, our data indicate that on a doped semiconductor photocatalyst, the positively or negatively charged microenvironment around trapped holes or electrons, respectively, greatly affects the electron transfer ability of the substrate and the binding or dissociation ability of substrate/product molecules at the $h^+/OH^\bullet$ or $e^-/O_2^{-\bullet}$ active sites. A charged microenvironment model has been used to explain the difference in properties of the two active sites around trapped electrons and holes. This model may also be applicable to several other semiconductor-based photocatalytic systems, such as Si-based catalysts.[36] The results obtained here improve our understanding of the nature of the two basic active sites in this semiconductor photocatalyst.

■ ASSOCIATED CONTENT

Ⓢ Supporting Information

Materials and methods, experimental details, and control experiments. This material is available free of charge via the Internet at http://pubs.acs.org.

■ AUTHOR INFORMATION

Corresponding Author

apalivisatos@lbl.gov

Notes

The authors declare no competing financial interest.

■ ACKNOWLEDGMENTS

Work on nanorod synthesis and single-molecule photocatalysis was funded by the Helios Solar Energy Research Center, which is supported by the Director, Office of Science, Office of Basic Energy Sciences of the U.S. Department of Energy under Contract DE-AC02-05CH11231. P.K.J. thanks the Miller Institute at UCB for his fellowship. B.J.B. was supported by a fellowship from the Department of Energy Office of Science Graduate Fellowship Program (DOE SCGF), made possible in part by the American Recovery and Reinvestment Act of 2009 and administered by ORISE−ORAU under Contract DE-AC05-06OR23100.

■ REFERENCES

(1) Fujishima, A.; Honda, K. *Nature* **1972**, *238*, 37.

(2) Ishibashi, K.-i.; Fujishima, A.; Watanabe, T.; Hashimoto, K. *Electrochem. Commun.* **2000**, *2*, 207.

(3) Ishibashi, K.-i.; Fujishima, A.; Watanabe, T.; Hashimoto, K. *J. Phys. Chem. B* **2000**, *104*, 4934.

(4) Ishibashi, K.-i.; Nosaka, Y.; Hashimoto, K.; Fujishima, A. *J. Phys. Chem. B* **1998**, *102*, 2117.

(5) Chen, X.; Liu, L.; Yu, P. Y.; Mao, S. S. *Science* **2011**, *331*, 746.

(6) Tachikawa, T.; Yamashita, S.; Majima, T. *J. Am. Chem. Soc.* **2011**, *133*, 7197.

(7) Tachikawa, T.; Wang, N.; Yamashita, S.; Cui, S.-C.; Majima, T. *Angew. Chem., Int. Ed.* **2010**, *49*, 8593.

(8) Grätzel, M. *Nature* **2001**, *414*, 338.

(9) Chen, X.; Mao, S. S. *Chem. Rev.* **2007**, *107*, 2891.

(10) Anpo, M.; Shima, T.; Kubokawa, Y. *Chem. Lett.* **1985**, 1799.

(11) Micic, O. I.; Zhang, Y.; Cromack, K. R.; Trifunac, A. D.; Thurnauer, M. C. *J. Phys. Chem.* **1993**, *97*, 13284.

(12) Nosaka, Y.; Natsui, H.; Sasagawa, M.; Nosaka, A. Y. *J. Phys. Chem. B* **2006**, *110*, 12993.

(13) Howe, R. F.; Grätzel, M. *J. Phys. Chem.* **1987**, *91*, 3906.

(14) Nakamura, R.; Imanishi, A.; Murakoshi, K.; Nakato, Y. *J. Am. Chem. Soc.* **2003**, *125*, 7443.

(15) Murakami, Y.; Kenji, E.; Nosaka, A. Y.; Nosaka, Y. *J. Phys. Chem. B* **2006**, *110*, 16808.

(16) Nosaka, Y.; Yamashita, Y.; Fukuyama, H. *J. Phys. Chem. B* **1997**, *101*, 5822.

(17) Hirakawa, T.; Nakaoka, Y.; Nishino, J.; Nosaka, Y. *J. Phys. Chem.* **1999**, *103*, 4399.

(18) Ishibashi, K. I.; Fujishima, A.; Watanabe, T.; Hashimoto, K. *J. Photochem. Photobiol., A* **2000**, *134*, 139.

(19) Naito, K.; Tachikawa, T.; Fujishima, A.; Majima, T. *J. Phys. Chem. C* **2008**, *112*, 1048.

(20) Edman, L.; Földes-Papp, Z.; Wennmalm, S.; Rigler, R. *Chem. Phys.* **1999**, *247*, 11.

(21) Naito, K.; Tachikawa, T.; Cui, S.-C.; Sugimoto, A.; Fujishima, A.; Majima, T. *J. Am. Chem. Soc.* **2006**, *128*, 16430.

(22) Hoffmann, M. R.; Martin, S. T.; Choi, W.; Bahnemann, D. W. *Chem. Rev.* **1995**, *95*, 69.

(23) Thompson, T. L.; Yates, J. T. Jr. *Chem. Rev.* **2006**, *106*, 4428.

(24) Chih, T.; Jao, H.-J.; Wang, C. O. *J. Electroanal. Chem.* **2005**, *581*, 159.

(25) Joo, J.; Kwon, S. G.; Yu, T.; Cho, M.; Lee, J.; Yoon, J.; Hyeon, T. *J. Phys. Chem. B* **2005**, *109*, 15297.

(26) Bechstein, R.; Kitta, M.; Schütte, J.; Onishi, H.; Kühnle, A. *Nanotechnology* **2009**, *20*, No. 264003.

(27) Valentin, C. D.; Pacchioni, G.; Onishi, H.; Kudo, A. *Chem. Phys. Lett.* **2009**, *469*, 166.

(28) Xu, W.; Kong, J. S.; Yeh, Y.-T. E.; Chen, P. *Nat. Mater.* **2008**, *7*, 992.

(29) Asahi, R.; Morikawa, T.; Ohwaki, T.; Aoki, K.; Taga, Y. *Science* **2001**, *293*, 269.

(30) del Río, L. A.; Fernández, V. M.; Rupérez, F. L.; Sandalio, L. M.; Palma, J. M. *Plant Physiol.* **1989**, *89*, 728.

(31) Gomes, A.; Fernandes, E.; Lima, J. L. F. C. *J. Biochem. Biophys. Methods* **2005**, *65*, 45.

(32) Xu, W.; Kong, J. S.; Chen, P. *J. Phys. Chem. C* **2009**, *113*, 2393.

(33) Moon, J.; Takagi, H.; Fujishiro, Y.; Awano, M. *J. Mater. Sci.* **2001**, *36*, 949.

(34) Redel, E.; Arsenault, E.; O'Brien, G. P.; Kherani, P. N.; Ozin, A. G. *Chem. Mater.* **2011**, *23*, 1353.

(35) Hurum, D. C.; Agrios, A. G.; Crist, S. E.; Gray, K. A.; Rajh, T.; Thurnauer, M. C. *J. Electron Spectrosc. Relat. Phenom.* **2006**, *150*, 155.

(36) Hou, Y.; Abrams, B. L.; Vesborg, P. C. K.; Björketun, M. E.; Herbst, K.; Bech, L.; Setti, A. M.; Damsgaard, C. D.; Pedersen, T.; Hansen, O.; Rossmeisl, J.; Dahl, S.; Nørskov, J. K.; Chorkendorff, I. *Nat. Mater.* **2011**, *10*, 434.